

Precoding Design for Multi-User MIMO Joint Communications and Sensing

Charlotte Muth , *Graduate Student Member, IEEE*, Shrinivas Chimmalgi ,
and Laurent Schmalen , *Fellow, IEEE*

Communications Engineering Lab (CEL), Karlsruhe Institute of Technology (KIT)
Hertzstr. 16, 76187 Karlsruhe, Germany, Email: first.last@kit.edu

Abstract—We investigate precoding for multi-user (MU) multiple-input multiple-output (MIMO) joint communications and sensing (JCAS) systems, taking into account the potential interference between sensing and communication channels. We derive indicators for the sensing and communication performance, i.e., the detection probability and the communication signal-to-interference-and-noise ratio (SINR) for general input signals. Our results show that the use of the communication signal for sensing can prevent a loss in communication performance if channel interference occurs, while the kurtosis of the transmit alphabet of the communication signal limits the sensing performance. We present simulation results of example setups.

Index Terms—Joint communications and sensing, Object detection, Higher-order modulation formats, MIMO

I. INTRODUCTION

Multiple-input multiple-output (MIMO) systems are fundamental to modern wireless communications, particularly in higher frequency bands where the increased path loss can be partially compensated through beamforming. MIMO enables spatial multiplexing, i.e., using spatial diversity to transmit multiple data streams simultaneously to improve spectral efficiency. Meanwhile, joint communications and sensing (JCAS) has gained significant attention due to its potential to support new functionalities, such as warning vehicles at a crossing from potential collision risks. In JCAS, sensing accuracy is closely linked to the available bandwidth, leading to higher frequency bands being considered for sensing [1].

A central challenge in JCAS lies in the design of transmit signals that effectively support both communications and sensing. While some research articles have proposed algorithms for precoding in multi-user (MU)-MIMO JCAS systems [2]–[4], the question of transmit signal design is an ongoing field of research. In [2], [5], potential sensing targets are illuminated using phase-modulated communication signals, which yield maximum signal-to-noise ratio (SNR) for object detection in single-input single-output systems. However, traditional communication systems often rely on higher-order quadrature amplitude modulation (QAM) formats to increase throughput, which degrades sensing performance. To

This work has received funding in part from the European Research Council (ERC) under the European Union's Horizon 2020 research and innovation programme (grant agreement No. 101001899) and in part from the German Federal Ministry of Research, Technology and Space (BMFTR) within the projects Open6GHub (grant agreement 16KISK010) and KOMSENS-6G (grant agreement 16KISK123).

flexibly trade off communication and sensing performance, constellation shaping has been proposed [6] for JCAS.

While a JCAS trade-off has been addressed for MIMO in multiple studies, they tend to address performance metrics such as side-lobe levels or image signal-to-interference-and-noise ratio (SINR) [7] which are related to the average detection probability or the Cramér-Rao bound (CRB) for parameter estimation [8]. Additionally, the communication signal streams use the same constellation and sensing is either done using communication signals or dedicated signals for sensing. We complement these results and methods by allowing communication signals of different constellations and directly optimizing the detection rate.

This work serves as a detailed analysis of the advantages and disadvantages of joint signaling or dedicated signals for sensing and investigates different scenarios. We obtain performance metrics, i.e., the target detection rate for a power detector and the communication SINR. Lastly, we investigate how communications are affected by interference caused by sensing signals.

II. SYSTEM MODEL

We consider a single-carrier monostatic MU MIMO JCAS system, where the transmitter and the sensing receiver are co-located at same base station with a uniform linear array (ULA) with K antennas and half-wavelength antenna spacing. Our goal is to detect a potential target based on the reflection of the transmitted signal at the target. Simultaneously, spatial multiplexing is used to communicate with N_{UE} UEs with a single antenna located at different positions than the sensing target. The sensing target is located randomly at an azimuth angle of $\theta \in [\theta_{\min}, \theta_{\max}]$. We consider multi-snapshot sensing with N_{block} samples and consider for simplicity single target detection. The system block diagram is illustrated in Fig. 1. Throughout this paper, deterministic scalars, vectors, and matrices are denoted by a , \mathbf{a} , and \mathbf{A} , respectively; random scalars, vectors, and matrices are denoted by \mathbf{a} , \mathbf{a} , and \mathbf{A} .

A. Transmitter

The communication transmitter generates the transmit bits for all UEs. We consider a transmit bit matrix $\mathbf{B} \in \{0, 1\}^{N_{\text{UE}} \times m}$, with $m = 4$ bits per symbol. The bits are mapped to symbols by the modulators, namely to N_{UE} normalized 16-QAM signals for each UE. Additionally, a

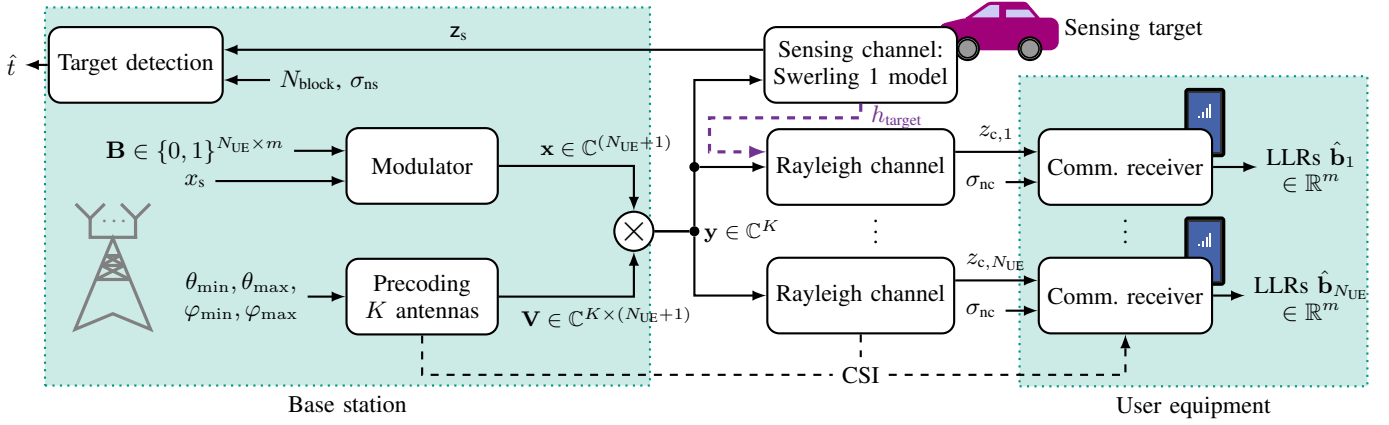


Fig. 1. JCAS system. The sensing target can become a reflector in the communication channel of user equipment (UE)1, introducing interference h_{target} .

constant-modulus signal x_s is generated for sensing, e.g. unit power samples with uniformly distributed phase, and concatenated to a transmit vector $\mathbf{x} \in \mathbb{C}^{N_{\text{UE}}+1}$. A linear precoder with weights $\mathbf{V} \in \mathbb{C}^{K \times (N_{\text{UE}}+1)}$ is used for beamforming. The modulator and beamformer employ power normalization. The transmit signal after linear precoding is

$$\mathbf{y} = \mathbf{V}\mathbf{x}. \quad (1)$$

B. Channels

A part of the radiated power is steered toward each UE by the precoder while another part is steered toward the sensing area of interest. The signal propagation from K antennas towards an azimuth angle φ is modeled with the spatial angle vector $\mathbf{a}_{\text{TX}}(\varphi) \in \mathbb{C}^K$ given by $\mathbf{a}_{\text{TX}}(\varphi) = (1, e^{j\pi \sin \varphi}, \dots, e^{j\pi(K-1) \sin \varphi})^\top$. For the communication part, the signal \mathbf{y} experiences Rayleigh fading. Signals transmitted at various angles of departure (AoDs) φ_u are received at the u th UE due to multipath propagation, as reflections from surrounding surfaces cause the signal to arrive from multiple directions. All reflections from $\varphi_u = (\varphi_{1u}, \varphi_{2u}, \dots)$ are assumed to arrive simultaneously at the UEs as spatial taps, i.e.

$$z_{c,u} = \sum_{d=1}^{\dim(\varphi_u)} \alpha_{c,d} \mathbf{a}_{\text{TX}}(\varphi_{du})^\top \mathbf{V} \mathbf{x} + n_{c,u}, \quad (2)$$

with fading coefficients $\alpha_{c,d} \sim \mathcal{CN}(0, \sigma_{c,d}^2)$, noise samples $n_{c,u} \sim \mathcal{CN}(0, \sigma_{nc}^2)$ and channel $\tilde{\mathbf{h}}_{c,du} := \alpha_{c,d} \mathbf{a}_{\text{TX}}(\varphi_{du})^\top \mathbf{V}$. To stress the importance of channel interference, we let the sensing target act as a reflective element within the channel of UE1 while additional user interference can be caused by precoding. We can rephrase (2) for UE1 as

$$\begin{aligned} z_{c,1} &= \sum_{d=1}^{\dim(\varphi_{u1})} \tilde{\mathbf{h}}_{c,d1} \mathbf{x} + n_c = \left(\sum_{u=1}^{N_{\text{UE}}+1} h_u x_u \right) + n_c \\ &= h_1 x_1 + \left(\sum_{u=2}^{N_{\text{UE}}} h_u x_u \right) + h_{\text{target}} \underbrace{x_{N_{\text{UE}}+1}}_{=x_s} + \underbrace{n_c}_{\text{noise}}, \end{aligned} \quad (3)$$

with $\mathbf{h} = (h_1, \dots, h_{N_{\text{UE}}+1}) = \sum_d \tilde{\mathbf{h}}_{c,d1}$ including precoding, fading, and additional multipath interference. We have rewritten the sensing interference as $h_{\text{target}} = h_{N_{\text{UE}}+1}$.

With $t \in \{0, 1\}$ indicating the presence of the target at an angle θ , we express the sensing signal reflected from said target in the monostatic setup as

$$\mathbf{z}_s = t \mathbf{a}_{\text{RX}}(\theta) \mathbf{a}_{\text{TX}}(\theta)^\top \mathbf{y} + \mathbf{n}_s, \quad (4)$$

with the radar target following a Swerling-1 model [9] with random variable $\mathbf{a} \sim \mathcal{CN}(0, \sigma_s^2)$ representing the radar cross section and path loss and noise $\mathbf{n}_s = (n_{s,1}, \dots, n_{s,K})$ with $n_{s,k} \sim \mathcal{CN}(0, \sigma_{ns}^2)$ and $k \in \{1, \dots, K\}$. The spatial angle vectors relate as $\mathbf{a}_{\text{RX}}(\theta) = \mathbf{a}_{\text{TX}}(\theta)$, with θ being the angle of departure (AoD) and angle of arrival (AoA) of the target. The radial velocity of the target is assumed to be zero, so no Doppler shift occurs.

C. Communication Receivers

The goal of the communication receiver is to recover the transmitted bits based on the received signal. We assume that channel estimation has already been performed at the communication receiver and that the precoding matrix \mathbf{V} is known. Therefore, full channel state information (CSI) is available at each UE to perform (MMSE) equalization. The demodulator outputs log-likelihood ratios (LLRs) $\hat{\mathbf{b}} \in \mathbb{R}^m$ that can be used as input to a soft decision channel decoder.

D. Sensing Receiver

We process N_{block} realizations of (4) for detection. With a Swerling-1 model, we model scan-to-scan deviations of the radar cross section (RCS), which manifest as a change in t during the observation window. Each realization also results in its own noise samples and transmit symbols. Therefore, we rewrite the samples of (4) for a time instance $\ell \in \{1, 2, \dots, N_{\text{block}}\}$ and antenna element k , with $c_\ell = \mathbf{a}_{\text{TX}}(\theta)^\top \mathbf{y}_\ell$ as

$$z_{s,k\ell} = t e^{j\pi(k-1) \sin \theta} a_\ell c_\ell + n_{s,k\ell}. \quad (5)$$

Although prior knowledge of the transmit signal or approximate target positions may be available in a monostatic sensing

scenario, in this work we assume that the transmit signal is unknown at the sensing receiver as well as the possible AoA of a target. This assumption provides a meaningful lower bound on performance when such information is available, while enabling closed-form expressions and analysis for the resulting detector.

A detector with false alarm probability P_f based on the Neyman-Pearson (NP) criterion [10] is given by

$$\frac{2}{\sigma_{\text{ns}}^2} \sum_{\ell=1}^{N_{\text{block}}} \sum_{k=1}^K |\mathbf{z}_{s,k\ell}|^2 \stackrel{\hat{t}=1}{\gtrless} Q_{\chi_{2K N_{\text{block}}}^2} (1 - P_f), \quad (6)$$

with $Q_{\chi_{2K N_{\text{block}}}^2}(\cdot)$ denoting the quantile function of a χ^2 distribution with $2K N_{\text{block}}$ degrees of freedom. Thus, if the left-hand side of (6) is higher than the detection threshold, a target is detected. Knowing the noise statistics, we can implement this power detector as a constant false alarm rate (CFAR) detector. This choice of detector enables us to analyze the detection statistics in closed form. For $t = 0$ only noise is present, yielding a χ^2 distribution. For $t = 1$ the detector input is influenced by beamforming and transmit signals, making the analysis more involved.

III. PERFORMANCE INDICATORS FOR SENSING AND COMMUNICATIONS

A. Detection Probability

The detector can be formulated in closed form using (6). We can drop the receive phase shift $e^{j\pi(k-1)\sin\theta}$ from (5), as only the received power is of interest. A single sample for the detector can be reformulated as

$$|\mathbf{z}_{s,k\ell}|^2 = |t \mathbf{c}_\ell \mathbf{a}_\ell + \mathbf{n}_{s,k\ell}|^2. \quad (7)$$

In the following, we derive a closed-form expression of the detector statistics for $t = 1$ to further analyze the impact of precoding on the detection probability.

Derivation: $\mathbf{n}_{s,k\ell}$ and \mathbf{a}_ℓ are independent circularly symmetric complex Gaussian random variables with zero mean and variances

$$\mathbb{E}\{|\mathbf{a}_\ell|^2\} = \sigma_s^2, \quad \mathbb{E}\{|\mathbf{n}_{s,k\ell}|^2\} = \sigma_{\text{ns}}^2.$$

Let $\mathbf{c}_\ell = \sum_{u=1}^{N_{\text{UE}}} \sqrt{\beta_u} \mathbf{x}_{u\ell}$ be fixed constants for now, with $\sqrt{\beta_u} = \mathbf{a}_{\text{TX}}(\theta)^\top (\mathbf{v})_u$ denoting the effects of beamforming. We keep the beamforming gain β_u constant by assuming approximately uniform illumination of sensing targets, otherwise the detection probability would be dependent on the AoA of the target. We want to derive the distribution of

$$\tilde{\mathbf{z}}_s = \sum_{\ell=1}^{N_{\text{block}}} \sum_{k=1}^K |\mathbf{z}_{s,k\ell}|^2 = \sum_{\ell=1}^{N_{\text{block}}} \sum_{k=1}^K |\mathbf{c}_\ell \mathbf{a}_\ell + \mathbf{n}_{s,k\ell}|^2 \quad (8)$$

to analyze the detector behavior. As \mathbf{c}_ℓ , \mathbf{a}_ℓ and $\mathbf{n}_{s,k\ell}$ are independently drawn from their respective distributions for each time sample ℓ , we focus on a single ℓ where we are interested in the distribution of $\sum_{k=1}^K |\mathbf{c}_\ell \mathbf{a}_\ell + \mathbf{n}_{s,k\ell}|^2$ with \mathbf{a}_ℓ being independent of k . The received samples for the K antennas are components of a multivariate distribution of a

variable $\mathbf{q} = [\mathbf{c}_\ell \mathbf{a}_\ell + \mathbf{n}_{s,1\ell}, \mathbf{c}_\ell \mathbf{a}_\ell + \mathbf{n}_{s,2\ell}, \dots, \mathbf{c}_\ell \mathbf{a}_\ell + \mathbf{n}_{s,K\ell}]^\top$. Then \mathbf{q} is a complex circular Gaussian with zero mean and covariance matrix

$$\Sigma_\ell = \sigma_{\text{ns}}^2 \mathbf{I} + |\mathbf{c}_\ell|^2 \sigma_s^2 \mathbf{1}_{K \times K}, \quad (9)$$

with all-one matrix $\mathbf{1}_{K \times K} \in \mathbb{C}^{K \times K}$. The covariance matrix Σ_ℓ is Hermitian positive-semi-definite and, hence, can be decomposed using the singular value decomposition as

$$\Sigma_\ell = \mathbf{U} \Lambda \mathbf{U}^H, \quad \Lambda = \text{diag}(\lambda_1, \dots, \lambda_K). \quad (10)$$

Let $\mathbf{r} = \mathbf{U}^H \mathbf{q}$ and, thus, since \mathbf{U} is unitary, $\mathbf{q} = \mathbf{U} \mathbf{r}$. Then $\mathbf{r} \sim \mathcal{CN}(\mathbf{0}, \Lambda)$, and all components $r_k \sim \mathcal{CN}(0, \lambda_k)$ are independent Gaussians. We can write

$$\sum_{k=1}^K |\mathbf{c}_\ell \mathbf{a}_\ell + \mathbf{n}_{s,k\ell}|^2 = \mathbf{q}^H \mathbf{q} = (\mathbf{U} \mathbf{r})^H (\mathbf{U} \mathbf{r}) = \sum_{k=1}^K |r_k|^2. \quad (11)$$

The variances λ_k of r_k are the eigenvalues of the covariance matrix Σ_ℓ . As Σ_ℓ is the sum of a diagonal matrix and a rank-1 matrix, the eigenvalues are known in closed form

$$\lambda_1 = \sigma_{\text{ns}}^2 + K |\mathbf{c}_\ell|^2 \sigma_s^2, \quad \lambda_2 = \dots = \lambda_K = \sigma_{\text{ns}}^2. \quad (12)$$

Knowing that $|r_k|^2$ follows an exponential distribution with rate parameter equal to $1/\lambda_k$ and that the moment-generating function (MGF) of the sum of independent variables is given by the product of the MGFs of the variables [11], the MGF of $\tilde{\mathbf{z}}_{s,\ell} = \sum_{k=1}^K |\mathbf{c}_\ell \mathbf{a}_\ell + \mathbf{n}_{s,k\ell}|^2$ is given by

$$M_{\tilde{\mathbf{z}}_{s,\ell}}(s) = \frac{1}{1 - (\sigma_{\text{ns}}^2 + K |\mathbf{c}_\ell|^2 \sigma_s^2)s} \left(\frac{1}{1 - \sigma_{\text{ns}}^2 s} \right)^{K-1}. \quad (13)$$

Given the independent time observations, the MGF of $\tilde{\mathbf{z}}_s = \sum_{\ell=1}^{N_{\text{block}}} \tilde{\mathbf{z}}_{s,\ell}$ is given by

$$M_{\tilde{\mathbf{z}}_s}(s) = \left(\frac{1}{1 - \sigma_{\text{ns}}^2 s} \right)^{(K-1)N_{\text{block}}} \cdot \prod_{\ell=1}^{N_{\text{block}}} \frac{1}{1 - (\sigma_{\text{ns}}^2 + K |\mathbf{c}_\ell|^2 \sigma_s^2)s}. \quad (14)$$

The probability density function (PDF) $f_{\tilde{\mathbf{z}}_s}(z)$ can be obtained from the MGF through the inverse Laplace transform

$$f_{\tilde{\mathbf{z}}_s}(z) = \mathcal{L}^{-1}\{M_{\tilde{\mathbf{z}}_s}(-s)\}. \quad (15)$$

Maximizing the detection probability, given by

$$P_d = \int_{\frac{\sigma_{\text{ns}}^2}{2} Q_{\chi_{2K N_{\text{block}}}^2} (1 - P_f)}^{\infty} f_{\tilde{\mathbf{z}}_s}(z) dz \quad (16)$$

requires either increasing the mean of $f_{\tilde{\mathbf{z}}_s}(z)$ or decreasing its variance. We calculate the mean and variance of the PDF in the presence of a target ($t = 1$) through the MGF, resulting in:

$$\begin{aligned} \mu &= \frac{d}{ds} M_{\tilde{\mathbf{z}}_s}(s=0) = KN_{\text{block}} \sigma_{\text{ns}}^2 + K \sigma_s^2 \left(\sum_{\ell=1}^{N_{\text{block}}} |\mathbf{c}_\ell|^2 \right) \\ &= KN_{\text{block}} \sigma_{\text{ns}}^2 + K \sigma_s^2 \sum_{\ell=1}^{N_{\text{block}}} \left| \sum_{u=1}^{N_{\text{UE}}} \sqrt{\beta_u} \mathbf{x}_{u\ell} \right|^2, \text{ and} \end{aligned} \quad (17)$$

$$\begin{aligned}
\sigma_{\tilde{z}_s}^2 &= \frac{d^2}{ds^2} M_{\tilde{z}_s}(s=0) - \mu^2 \\
&= N_{\text{block}} K \sigma_{\text{ns}}^4 + K^2 \sigma_s^4 \sum_{\ell=1}^{N_{\text{block}}} \left| \sum_{u=1}^{N_{\text{UE}}+1} \sqrt{\beta_u} x_{u\ell} \right|^4 \\
&\quad + 2K \sigma_{\text{ns}}^2 \sigma_s^2 \sum_{\ell=1}^{N_{\text{block}}} \left| \sum_{u=1}^{N_{\text{UE}}+1} \sqrt{\beta_u} x_{u\ell} \right|^2. \tag{18}
\end{aligned}$$

We now consider the transmit symbols as random variables $\mathbf{x} \in \mathbb{C}^{N_{\text{UE}}+1} \sim P_{\mathbf{x}}$. For sufficiently large N_{block} , we can apply the law of large numbers over N_{block} and constrain the launch power using $\mathbb{E}_{P_{\mathbf{x}}}\{|\mathbf{x}|^2\} = 1$ (i) and $\sum_{u=1}^{N_{\text{UE}}+1} |\beta_u| = 1$ (ii) with $\mathbb{E}_{P_{\mathbf{x}}}\{\mathbf{x}\} = 0$ (iii). If the signals for different UEs are uncorrelated, we can approximate:

$$\begin{aligned}
\lambda &:= \mathbb{E}_{P_{\mathbf{x}}} \left\{ \left| \sum_{u=1}^{N_{\text{UE}}+1} \sqrt{\beta_u} x_u \right|^2 \right\} \\
&= |\beta_1| \mathbb{E}_{P_{\mathbf{x}}} \{ |x_1|^2 \} + \dots + \mathbb{E}_{P_{\mathbf{x}}} \left\{ 2 \operatorname{Re}\{ \sqrt{\beta_1 \beta_2^*} x_1 x_2^* \} \right\} \\
&= \sum_{u=1}^{N_{\text{UE}}+1} |\beta_u| = 1 \tag{19} \\
\tilde{\kappa} &:= \mathbb{E}_{P_{\mathbf{x}}} \left\{ \left| \sum_{u=1}^{N_{\text{UE}}+1} \sqrt{\beta_u} x_u \right|^4 \right\} \\
&= |\beta_1|^2 \underbrace{\mathbb{E}_{P_{\mathbf{x}}} \{ |x_1|^4 \}}_{\kappa_1} + \dots + 4|\beta_1||\beta_2| + \dots \\
&\stackrel{(ii)}{=} \sum_{u=1}^{N_{\text{UE}}+1} |\beta_u|^2 \kappa_u + 2|\beta_u|(1 - |\beta_u|), \tag{20}
\end{aligned}$$

with kurtosis κ_u of x_u . Then, (17) and (18) can be approximated as

$$\begin{aligned}
\mu &\approx K N_{\text{block}} (\sigma_{\text{ns}}^2 + \sigma_s^2) \\
\sigma_{\tilde{z}_s}^2 &\approx N_{\text{block}} K (\sigma_{\text{ns}}^4 + K \sigma_s^4 \tilde{\kappa} + 2\sigma_{\text{ns}}^2 \sigma_s^2).
\end{aligned}$$

B. Influence of Precoding

As stated before, the detection performance can be maximized through increasing μ or decreasing $\sigma_{\tilde{z}_s}^2$. The detection probability within the constraints (i) – (iii) is affected by the transmit signal and beamforming only through $\tilde{\kappa}$ given by (20). The larger the variance of the distribution, the lower a potential detection rate becomes. For fixed constellations $P_{\mathbf{x}}$ and \mathbf{x} , we compute the Hessian matrix of $\tilde{\kappa}(|\beta_1|, \dots, |\beta_{N_{\text{UE}}+1}|)$ as

$$\mathbf{H}_{\tilde{\kappa}} = \begin{pmatrix} 2\kappa_1 - 4 & \dots & 0 \\ \vdots & \ddots & \vdots \\ 0 & \dots & 2\kappa_{N_{\text{UE}}+1} - 4 \end{pmatrix}. \tag{21}$$

For any vector $\mathbf{w} \in \mathbb{R}^{N_{\text{UE}}+1}$,

$$\mathbf{w}^\top \mathbf{H}_{\tilde{\kappa}} \mathbf{w} = \sum_{u=1}^{N_{\text{UE}}+1} w_u^2 (2\kappa_u - 4) \leq 0, \tag{22}$$

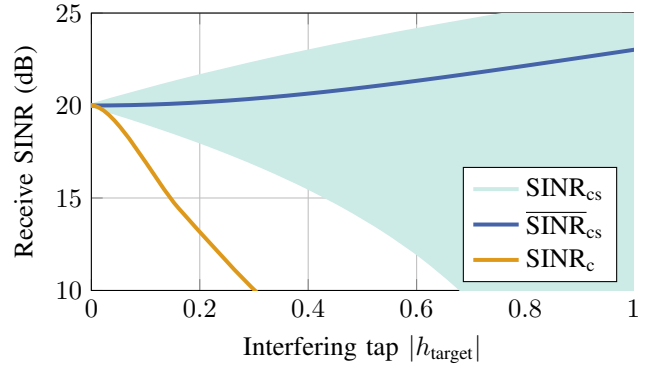


Fig. 2. Communication SINR with $\text{SNR}_c = 20 \text{ dB}$ and $h_1 = 1$.

as $1 \leq \kappa_u \leq 2$ for realistic constellation kurtosis. If $\kappa_u = 2$ for all u , which applies for Gaussian distributed constellation points, $\tilde{\kappa}$ is affine and the choice of $|\beta_u|$ becomes irrelevant, leading to identical performance. In all other cases, $\mathbf{H}_{\tilde{\kappa}}$ is negative definite and $\tilde{\kappa}$ is strictly concave with respect to $|\beta_u|$. Then, the minima of $\tilde{\kappa}$ can be found at the boundaries of the feasible set, with the global minimum at

$$|\beta_u| = \begin{cases} 1, & u = \arg \min_u \kappa_u \\ 0, & \text{otherwise.} \end{cases} \tag{23}$$

In words, the detection probability is maximized if the target is illuminated only by the signal with the lowest κ_u .

C. Communications SINR

The SINR for communication, using normalized constellations is given by

$$\text{SINR}_c = \frac{|h_1|^2}{\sum_{u=2}^{N_{\text{UE}}} |h_u|^2 + |h_{\text{target}}|^2 + \sigma_{\text{nc}}^2}. \tag{24}$$

To analyze the effect of channel interference, we examine the case where the signal for UE1 illuminates the sensing area resulting in signal $x_s = x_1$. Then, the SINR is

$$\text{SINR}_{\text{cs}} = \frac{|h_1 + h_{\text{target}}|^2}{\sum_{u=2}^{N_{\text{UE}}} |h_u|^2 + \sigma_{\text{nc}}^2}. \tag{25}$$

Depending on the phase difference $\phi = \angle h_1 - \angle h_{\text{target}}$ which we assume to be uniformly distributed, the resulting SINR can be higher or lower compared to (24). We obtain the mean SINR as

$$\begin{aligned}
\overline{\text{SINR}}_{\text{cs}} &= \frac{\int_{-\pi}^{\pi} (|h_1|^2 + |h_{\text{target}}|^2 + 2 \operatorname{Re}\{ |h_1 h_{\text{target}}| e^{i\phi} \}) d\phi}{2\pi \left(\sum_{u=1}^{N_{\text{UE}}} |h_u|^2 + \sigma_{\text{nc}}^2 \right)} \\
&= \frac{|h_1|^2 + |h_{\text{target}}|^2}{\sum_{u=2}^{N_{\text{UE}}} |h_u|^2 + \sigma_{\text{nc}}^2}.
\end{aligned} \tag{26}$$

Fig. 2 displays the possible SINR range and average SINR resulting from separate signaling for sensing or reuse of a communication signal. Even if additional interference from a sensing signal is not phase-coherent, $\overline{\text{SINR}}_{\text{cs}}$ actually rises with increased interference $|h_{\text{target}}|$. In a scenario where interference is caused by reflections in the environment, we cannot expect the signals to have the same phase, so this is an encouraging result from a communications perspective.

IV. SIMULATION SETUP

We train an autoencoder (AE) framework similar to [12] with precoding and demodulation implemented as neural networks (NNs)¹. A weight parameter $w_s \in [0, 1]$ controls the impact of the detection task, resulting in the loss

$$L = (1 - w_s)L_{\text{comm}} + w_sL_{\text{detect}}, \quad (27)$$

with the loss terms given by

$$L_{\text{comm}} = -\sum_{u=1}^{N_{\text{UE}}} \log \left(\sum_{i=1}^m 1 - H(b_{iu} || \hat{b}_{iu}) \right), \quad L_{\text{detect}} = H(t || \hat{t}),$$

with $H(\cdot || \cdot)$ denoting the binary cross entropy between two binary distributions. The communication loss is a reformulated utility function, leading to maximum fairness [13].

Minimizing L_{detect} corresponds to maximizing the detection probability (16). As shown in Sec. III-A, the detection probability is maximized when $\tilde{\kappa}$ is minimized. As $\tilde{\kappa}$ is concave with respect to resource allocation, gradient descent will lead to illumination of the sensing area by whichever signal is initially strongest. Therefore, it is particularly sensitive to the initialization. To incentivize convergence to the global minimum, we initialize \mathbf{V} such that $\tilde{\kappa}$ is maximum.

V. RESULTS AND DISCUSSION

We simulate two UEs at AoAs of $\varphi = \{50^\circ, 70^\circ\}$. A potential radar target is located in a range $\theta \in [-20^\circ, 20^\circ]$. For transmission and sensing, we simulate a ULA with $K = 16$ and we consider an observation window of $N_{\text{block}} = 15$. For the sensing receiver, we set the false alarm rate to $P_f = 10^{-2}$. The signal power is $\sigma_c^2 = 1$ and noise power $\sigma_{\text{nc}}^2 = 0.01$ for both UEs and we train a respective decoder. We set $w_s = 0.2$ and vary the amount of interference for targets with $\theta \in [10^\circ, 20^\circ]$ to UE1 by varying $h_{\text{target}}/c \sim \mathcal{N}(0, \sigma_{c,\text{target}}^2)$. We compare three different cases for the sensing receiver:

- $\tilde{z}_{s,\text{CM}}$ describes sensing using only a constant modulus phase-modulated signal x_s for sensing.
- $\tilde{z}_{s,\text{QAM}}$ describes sensing using the communication 16-QAM signals $x_1, \dots, x_{N_{\text{UE}}}$.
- $\tilde{z}_{s,\text{QAM+CM}}$ allows for a combination of a dedicated sensing signal x_s and communication signals $x_1, \dots, x_{N_{\text{UE}}}$.

A. Detector Statistics

In Fig. 3, the empirical histograms, the PDFs obtained from (15) and the detection threshold are shown for the case of no target ($t = 0$) and a target illuminated by a 16-QAM signal ($t = 1$). We obtained the PDFs by generating 50 realizations for each $|c_l|$, calculating the mean of $M_{\tilde{z}_s}(s)$ and then applying the numerical inverse Laplace transform. As the Laplace transform is a linear transform, this is equivalent to the mean PDF. The histograms and PDFs match very well. For smaller noise power σ_{ns}^2 , both PDFs shift to the left and become more narrow. A larger signal power σ_s^2 results in the PDF for $t = 1$ being shifted to the right and widened.

¹Code at <https://github.com/frozenhairdryer/JCAS-MIMO-precoding>

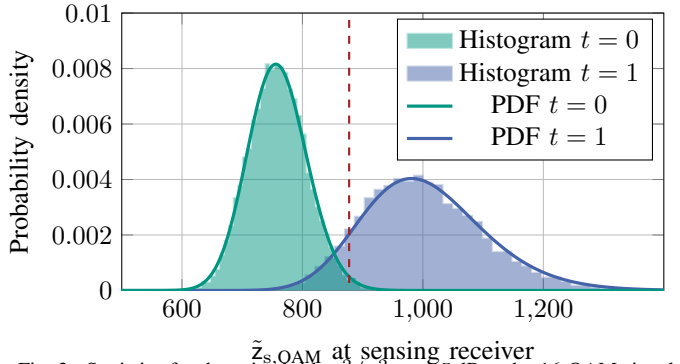


Fig. 3. Statistics for detection with $\sigma_s^2/\sigma_{\text{ns}}^2 = -5$ dB and a 16-QAM signal. The dashed line indicates the detection threshold for $P_f = 0.01$.

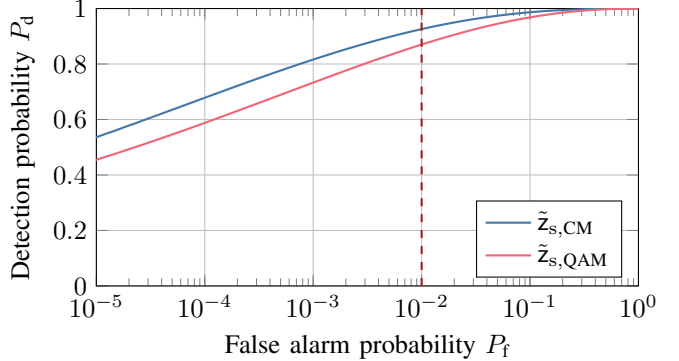


Fig. 4. Detection probability with $\sigma_s^2/\sigma_{\text{ns}}^2 = -5$ dB for phase-modulated and 16-QAM sensing input. The dashed line indicates the operating point of $P_f = 0.01$ used for further evaluation.

In the case of independent channels for sensing and communication, we get optimal sensing performance if a dedicated constant-modulus signal is used for sensing. In Fig. 4, P_d for changing P_f based on (15) is shown. The detector performs consistently better under $\tilde{z}_{s,\text{CM}}$, as the signal has a lower kurtosis κ than $\tilde{z}_{s,\text{QAM}}$. For very high false alarm rates this gap can vanish.

B. Precoding Evaluation

Trained beam patterns for the different approaches are shown in Fig. 5. For $\tilde{z}_{s,\text{CM}}$ resulting from $\sigma_{c,\text{target}} = 0$, the whole area of interest for sensing is illuminated by the constant modulus sensing signal. For $\sigma_{c,\text{target}} \geq 0.08$, the beam pattern switches to $\tilde{z}_{s,\text{QAM+CM}}$, as the section causing

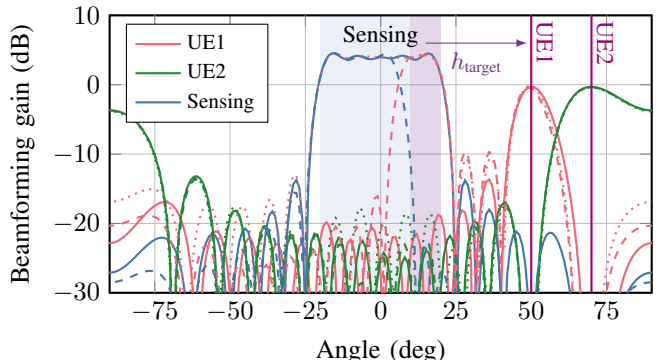


Fig. 5. Beam patterns for two UEs using 16-QAM with example scenarios $\tilde{z}_{s,\text{CM}}$, $\tilde{z}_{s,\text{QAM+CM}}$, and $\tilde{z}_{s,\text{QAM}}$.

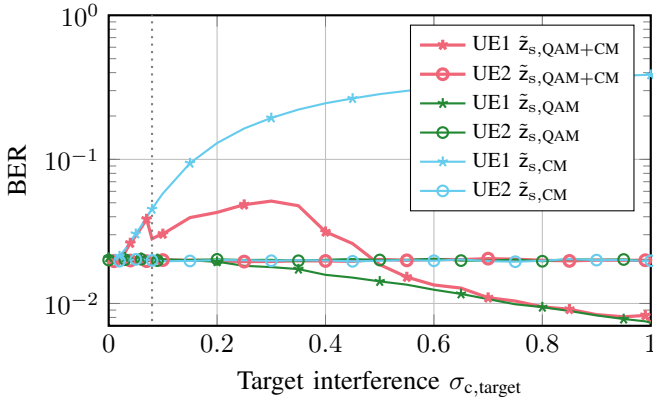


Fig. 6. BER at $\text{SNR}_c = 20 \text{ dB}$ for 2 UEs using 16-QAM for modulation and the beam patterns of Fig. 5 for different target interference at UE1.

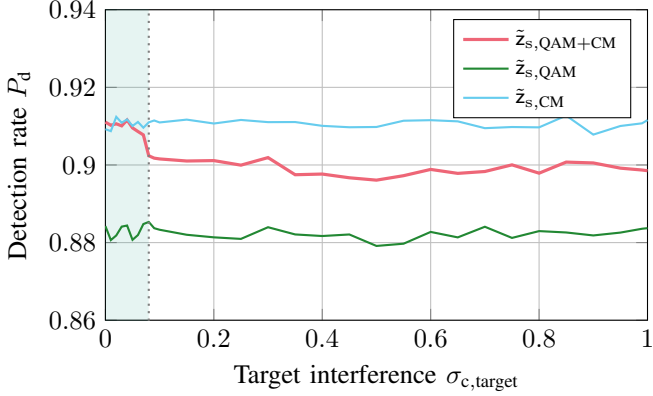


Fig. 7. Detection rate with varied interference. The interfering sensing area is illuminated by the sensing signal in $\boxed{\text{---}}$ and by a beam of the communication signal of UE1 otherwise.

interference is illuminated with the signal of UE1. For $\tilde{z}_{s,\text{QAM}}$, the signal of UE1 illuminates the whole sensing area.

Concerning communication performance, the bit error rate (BER) for $t = 1$ and the target being at angle $\theta \in [10^\circ, 20^\circ]$ is shown in Fig. 6. The BER for UE2 remains constant. For UE1, the BER associated with $\tilde{z}_{s,\text{QAM+CM}}$ rises first because the whole (for $\sigma_{c,\text{target}} < 0.08$) or part of the interfering area is illuminated by the constant-modulus signal, reducing the SINR. With $\sigma_{c,\text{target}} > 0.6$, the target is illuminated by the 16-QAM signal only, approaching the performance of $\tilde{z}_{s,\text{QAM}}$. For $\tilde{z}_{s,\text{QAM}}$, the BER for UE1 decreases slowly. If the whole sensing area is consistently illuminated with a constant-modulus signal in scenario $\tilde{z}_{s,\text{CM}}$, the BER of UE1 increases significantly with increasing $\sigma_{c,\text{target}}$. These findings match the expectations from Fig. 2.

Finally, we evaluate the detection rate based on $\sigma_{c,\text{target}}$ in Fig. 7. If only $\tilde{z}_{s,\text{QAM}}$ or $\tilde{z}_{s,\text{CM}}$ are used, the detection rate remains constant independently of $\sigma_{c,\text{target}}$, representing reference points for the achievable detection rate. Using $\tilde{z}_{s,\text{QAM+CM}}$, we clearly see a decrease of the detection rate when the illumination source of the interfering area switches to the communication signal at $\sigma_{c,\text{target}} = 0.08$. The detection rate decreases slightly further and stabilizes around $P_d \approx 0.9$.

To summarize, if significant interference occurs it is vital to perform sensing of spatially interfering components with

a communication signal.

VI. CONCLUSION

In this paper, we provide guidance on how to design the transmit signal for MIMO JCAS systems based on the interference between sensing and communication channels. Areas of interest for sensing can be divided into sections that cause user interference for communication users and non-interfering sections and be handled separately as follows: If there is no interference, using a constant-modulus signal for sensing leads to optimal target detection without influencing communication performance. If interference is observed, we encounter a trade-off. Using a communication signal for sensing aids in communication performance, but depending on the kurtosis of the used communication signal the sensing performance is limited. Using the sum of two or more different signals for sensing is not recommended, as it leads to worse target detection than using a single signal. The kurtosis of transmit signals being a major trade-off parameter for JCAS remains consistent with the literature.

REFERENCES

- [1] J. A. Zhang, M. L. Rahman, K. Wu, X. Huang, Y. J. Guo, S. Chen, and J. Yuan, "Enabling joint communication and radar sensing in mobile networks—a survey," *Commun. Surveys Tuts.*, vol. 24, no. 1, pp. 306–345, 2022.
- [2] P. Wang, Y. Cao, W. Ni, and D. Han, "Pareto-optimal waveform design for multi-user and multi-target mimo-isac systems," in *2024 IEEE Int. Conf. Acoustics, Speech, and Signal Process. Workshops*, 2024, pp. 219–223.
- [3] F. Dong, W. Wang, X. Li, F. Liu, S. Chen, and L. Hanzo, "Joint beamforming design for dual-functional MIMO radar and communication systems guaranteeing physical layer security," *IEEE Trans. Green Commun. and Netw.*, vol. 7, no. 1, pp. 537–549, mar 2023.
- [4] N. T. Nguyen, V.-D. Nguyen, H. V. Nguyen, H. Q. Ngo, A. L. Swindlehurst, and M. Juntti, "Performance analysis and power allocation for massive MIMO ISAC systems," *IEEE Trans. on Signal Process.*, vol. 73, pp. 1691–1707, 2025.
- [5] C. Ouyang, Y. Liu, and H. Yang, "MIMO-ISAC: Performance analysis and rate region characterization," *IEEE Wireless Commun. Lett.*, vol. 12, no. 4, pp. 669–673, 2023.
- [6] B. Geiger, F. Liu, S. Lu, A. Rode, and L. Schmalen, "Joint optimization of geometric and probabilistic constellation shaping for OFDM-ISAC systems," in *Proc. IEEE Int. Symposium Joint Commun. Sensing*, Oulu, Finland, Jan. 2025.
- [7] M. F. Keskin, M. M. Mojahedian, J. O. Lacruz, C. Marcus, O. Eriksson, A. Giorgetti, J. Widmer, and H. Wymeersch, "Fundamental trade-offs in monostatic isac: A holistic investigation toward 6g," *IEEE Trans. Wireless Commun.*, vol. 24, no. 9, pp. 7856–7873, 2025.
- [8] H. Hua, T. X. Han, and J. Xu, "Mimo integrated sensing and communication: Crb-rate tradeoff," *IEEE Trans. Wireless Commun.*, vol. 23, no. 4, pp. 2839–2854, Apr. 2024.
- [9] P. Swerling, "Probability of detection for fluctuating targets," *IEEE Trans. Inf. Theory*, vol. 6, no. 2, pp. 269–308, Apr. 1960.
- [10] H. L. van Trees, *Optimum Array Processing: Part IV of Detection, Estimation, and Modulation Theory*. Wiley, 2002.
- [11] K.-H. Pho, T. D.-C. Ho, T.-K. Tran, and W.-K. Wong, "Moment generating function, expectation and variance of ubiquitous distributions with applications in decision sciences: A review," *Advances in Decision Sciences*, vol. 23, no. 2, pp. 1–85, 2019.
- [12] C. Muth, B. Geiger, D. G. Gaviria, and L. Schmalen, "Neural network-based single-carrier joint communication and sensing: loss design, constellation shaping and precoding," *IEEE Access*, Sep. 2025.
- [13] E. Castaneda, A. Silva, A. Gameiro, and M. Kountouris, "An overview on resource allocation techniques for multi-user MIMO systems," *IEEE Commun. Surveys Tuts.*, vol. 19, no. 1, pp. 239–284, Mar. 2017.